International Journal of Heat and Mass Transfer 52 (2009) 760–766

Contents lists available at ScienceDirect

International Journal of Heat and Mass Transfer

journal homepage: www.elsevier.com/locate/ijhmt

Modeling of the heat transfer and flow features of the thermal plasma reactor with counter-flow gas injection

Gui-Qing Wu [a], He-Ping Li [a,*], Cheng-Yu Bao [a], Xi Chen [b]

[a] Department of Engineering Physics, Tsinghua University, Beijing 100084, PR China
[b] Department of Engineering Mechanics, Tsinghua University, Beijing 100084, PR China

ARTICLE INFO

Article history:
Received 11 December 2007
Received in revised form 10 July 2008
Available online 24 September 2008

Keywords:
Thermal plasma
Reactor
Modeling
Counter-flow injection
Swirling effect

ABSTRACT

Modeling study is conducted to reveal the heat transfer and flow features of the thermal plasma reactor with a counter-flow gas injection and used for nano-particle synthesis. The modeling results show that a variety of parameters, such as the temperature and flow rate of the carrier gas, the operation conditions of the plasma torch, the distance between the plasma torch exit and the carrier-gas injector exit, the swirling of the plasma jet or the carrier gas, etc., can all affect appreciably the temperature and flow fields and the locations of the stagnation layers formed in the plasma reactor. An appropriate combination of the operation parameters of the reactor is thus required in order to obtain a suitable stagnation layer for the synthesis of nano-scale particles.

1. Introduction

Due to their outstanding features with rather high specific enthalpy and thermal conductivity, thermal plasmas have been used widely in the fields of advanced materials processing, e.g., plasma spraying, particle spheroidization, synthesis of micro- or nano-scale particles, etc., in last decades [1,2]. In the synthesis of micro- or nano-scale particles, the raw materials are usually fed into the plasma region with the help of cold carrier-gas injected laterally (or in the direction perpendicular to the plasma jet axis), then the materials are heated, melted, evaporated, dissociated/decomposed, synthesized in the plasma region, and finally the fine powders with appropriate size distributions are obtained. Compared to the traditional plasma reactors with lateral carrier-gas injection, the plasma reactor with counter injection of the cold fluid (gas or liquid) can improve the reaction environment significantly, such as enhancing the residence time of the reactants in the hot core region, stimulating the intimate mixing of reactants with the plasma, and controlling the particle sizes by reducing particle coagulation or coalescence, etc. In early 1990s, a counter-flow liquid injection plasma reactor for synthesis of advanced ceramic powders was developed in the High Temperature and Plasma Laboratory of the University of Minnesota [3,4]. In recent years, the plasma reactor has been employed for synthesizing aluminum nano-particles with counter-injection of pre-heated carrier-gas (argon) and $AlCl_3$ vapor with temperature in the range of 165–180 °C [5].

In Refs. [3,4], experimental and modeling studies were conducted concerning the characteristics of the laminar thermal plasma reactor with counter-injected liquid feedstock. Those studies showed that many parameters, such as the operation parameters of the plasma torch (e.g., the input power, the working-gas flow rate, etc.), the distance between the plasma torch exit and the injector exit, the swirling of the plasma jet, etc., could appreciably influence the temperature and flow fields in the counter-injection plasma reactor, as well as the particle size distributions. In Ref. [5], an experimental study on the characteristics of nano-scale aluminum particles synthesized within a counter-flow gas-mixture (argon and $AlCl_3$ vapor) plasma reactor were conducted. However, so far no systematic modeling study is performed on the heat transfer and flow features of the plasma reactor with counter-injected carrier gas, as employed in Ref. [5]. In order to obtain a favorable environment for controlling the size distributions of the synthesized particles or optimizing the reactor operation parameters, it is essential to study the heat transfer and flow patterns within the plasma reactor, and to understand the complicated physical/chemical processes occurring in the vicinity of the stagnation layer formed between the plasma torch exit and the injector exit [2,5].

In this paper, a two-dimensional simulation is conducted concerning the influences of reactor operation parameters, such as the input power and working-gas flow rate of the plasma torch, the flow rate and temperature of the carrier gas, the distance between the plasma torch exit and the carrier-gas injector exit and the swirling at the plasma jet side or the carrier gas side, on the heat transfer and flow features of the thermal plasma reactor with counter-flow gas injection, as shown in Fig. 1.

* Corresponding author. Tel./fax: +86 10 6278 2816.
E-mail address: liheping@tsinghua.edu.cn (H.-P. Li).

0017-9310/$ - see front matter © 2008 Elsevier Ltd. All rights reserved.
doi:10.1016/j.ijheatmasstransfer.2008.07.043

Nomenclature

c_p	specific heat at constant pressure (J kg^{-1} K^{-1})
c_1, c_2, c_μ, σ_K, σ_ε	turbulence model constants
G	turbulent generation term (W m^{-3})
h	specific enthalpy (J kg^{-1})
K	turbulent kinetic energy (m^2 s^{-2})
k	thermal conductivity (W m^{-1} K^{-1})
L	distance between plasma torch and injector exit (m)
M	momentum of the plasma jet or the carrier gas (kg m s^{-2})
P	torch power (W)
p	gas pressure (Pa)
Pr_t	turbulent Prandtl number
Q	flow rate of the gas (m^3 s^{-1})
R_{in}	inner radius of the torch nozzle or the carrier-gas injector (m)
R_M	momentum ratio
R_{out}	outer radius of the calculation domain (m)
S	swirl number
S_R	radiation power per unit gas volume (W m^{-3})
T	temperature (K)
v_{01}, v_{02}	maximum absolute value of the axial velocity component at the torch exit or the injector inlet (m s^{-1})
$v_{\theta m}$, R_s	maximum value of the tangential velocity component and its radial location (m s^{-1}, m)
v_z, v_r, v_θ	velocity components in z-, r-, and θ-directions (m s^{-1})
z, r, θ	coordinate in axial, radial or tangential direction

Greek symbols

ε	turbulent kinetic-energy dissipation rate (m^2 s^{-3})
η	thermal efficiency of the plasma torch
λ	distance between stagnation point and plasma torch exit (m)
μ	molecular viscosity (Pa s)
μ_t	turbulent viscosity (Pa s)
ρ	mass density (kg m^{-3})
ξ	dimensionless distance ($\xi = \lambda/L$)
Γ	effective diffusion coefficient

Subscripts

car, 2	carrier gas
in	input or value at the inner side
m, 0	maximum value
M	momentum
out	output or value at the outer side
p, 1	plasma
s	inner point of the solid wall
t	turbulent
w	wall
z, r, θ	components in z-, r-, and θ-directions

2. Modeling approach

2.1. Assumptions

Main assumptions employed in this study include that (1) the flow within the plasma reactor is axi-symmetric, quasi-steady, turbulent and at atmospheric pressure; (2) gas properties are temperature-dependent; (3) the plasma is optically thin and in the local thermodynamic equilibrium (LTE) state; (4) the viscous dissipation and the pressure work terms in the energy equation are negligible; and (5) argon is used as the plasma forming-gas and the carrier gas, i.e., the small amount of $AlCl_3$ vapor in the gas mixture is not considered in this study for simplicity.

2.2. Governing equations

Based on the preceding assumptions, the governing equations used in this modeling can be written in the cylindrical coordinates (r, z, θ) as follows:

Continuity equation:

$$\frac{1}{r}\frac{\partial}{\partial r}(r\rho v_r) + \frac{\partial}{\partial z}(\rho v_z) = 0 \tag{1}$$

Momentum conservation equation (z-direction):

$$\frac{\partial(\rho v_z v_z)}{\partial z} + \frac{1}{r}\frac{\partial(r\rho v_z v_r)}{\partial r} = -\frac{\partial p}{\partial z} + \frac{1}{r}\frac{\partial}{\partial r}\left[\Gamma_u r\left(\frac{\partial v_z}{\partial r} + \frac{\partial v_r}{\partial z}\right)\right] + 2\frac{\partial}{\partial z}\left(\Gamma_u \frac{\partial v_z}{\partial z}\right) \tag{2}$$

Momentum conservation equation (r-direction):

$$\frac{\partial(\rho v_z v_r)}{\partial z} + \frac{1}{r}\frac{\partial(r\rho v_r v_r)}{\partial r} = -\frac{\partial p}{\partial r} + \frac{2}{r}\frac{\partial}{\partial r}\left(r\Gamma_u \frac{\partial v_r}{\partial r}\right) + \frac{\partial}{\partial z}\left[\Gamma_u\left(\frac{\partial v_r}{\partial z} + \frac{\partial v_z}{\partial r}\right)\right] - 2\Gamma_u \frac{v_r}{r^2} + \rho\frac{(rv_\theta)^2}{r^3} \tag{3}$$

Momentum conservation equation (θ-direction):

$$\frac{\partial(r\rho v_z v_\theta)}{\partial z} + \frac{1}{r}\frac{\partial(r^2\rho v_r v_\theta)}{\partial r} = \frac{\partial}{\partial z}\left[\Gamma_u \frac{\partial(v_\theta r)}{\partial z}\right] + \frac{1}{r}\frac{\partial}{\partial r}\left[\Gamma_u r\frac{\partial(v_\theta r)}{\partial r}\right] - \frac{2}{r}\frac{\partial(r\Gamma_u v_\theta)}{\partial r} \tag{4}$$

Energy conservation equation:

$$\frac{\partial(\rho v_z h)}{\partial z} + \frac{1}{r}\frac{\partial(r\rho v_r h)}{\partial r} = \frac{\partial}{\partial z}\left(\Gamma_h \frac{\partial h}{\partial z}\right) + \frac{1}{r}\frac{\partial}{\partial r}\left(r\Gamma_h \frac{\partial h}{\partial r}\right) - S_R \tag{5}$$

In this paper, the standard K–ε two-equation turbulence model is employed to study the influence of turbulence on the heat transfer and flow patterns within the plasma reactor. The corresponding turbulent kinetic energy and its dissipation rate equations are as follows:

$$\frac{\partial}{\partial z}(\rho v_z K) + \frac{1}{r}\frac{\partial}{\partial r}(\rho v_r r K) = \frac{\partial}{\partial z}\left(\Gamma_K \frac{\partial K}{\partial z}\right) + \frac{1}{r}\frac{\partial}{\partial r}\left(r\Gamma_K \frac{\partial K}{\partial r}\right) + G - \rho\varepsilon \tag{6}$$

$$\frac{\partial}{\partial z}(\rho v_z \varepsilon) + \frac{1}{r}\frac{\partial}{\partial r}(\rho v_r r\varepsilon) = \frac{\partial}{\partial z}\left(\Gamma_\varepsilon \frac{\partial \varepsilon}{\partial z}\right) + \frac{1}{r}\frac{\partial}{\partial r}\left(r\Gamma_\varepsilon \frac{\partial \varepsilon}{\partial r}\right) + \frac{\varepsilon}{K}(c_1 G - c_2\rho\varepsilon) \tag{7}$$

In Eqs. (1)–(7), z, r and θ are the axial, radial and tangential coordinates, while v_z, v_r and v_θ are the velocity components in the z-, r- and θ-directions, respectively. ρ, h and p are the mass density, specific enthalpy and pressure of argon, K and ε are the turbulent kinetic energy and its dissipation rate, and S_R is the temperature-dependent radiation power per unit volume of the argon plasma.

The turbulence generation term, G, appearing in Eqs. (6) and (7) is expressed as

$$G = \mu_t\left\{2\left[\left(\frac{\partial v_z}{\partial z}\right)^2 + \left(\frac{\partial v_r}{\partial r}\right)^2 + \left(\frac{v_r}{r}\right)^2\right] + \left(\frac{\partial v_z}{\partial r} + \frac{\partial v_r}{\partial z}\right)^2 + \left(\frac{\partial v_\theta}{\partial z}\right)^2 + \left(\frac{\partial v_\theta}{\partial r} - \frac{v_\theta}{r}\right)^2\right\} \tag{8}$$

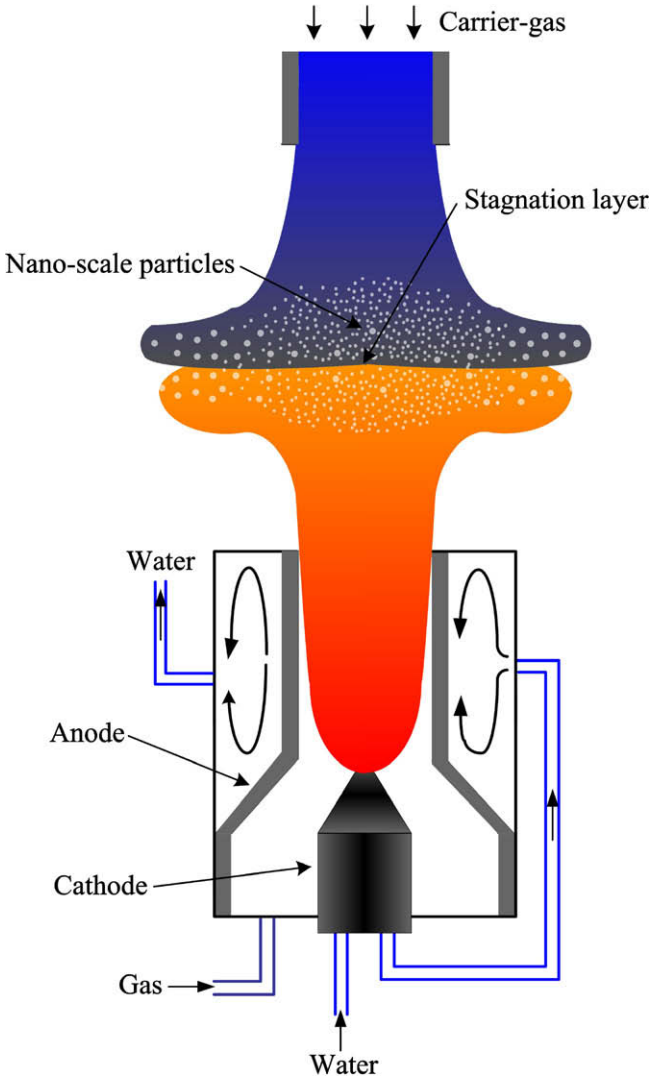

Fig. 1. Schematic diagram of the thermal plasma reactor with the counter injection of the carrier gas.

All the physical quantities in Eqs. (1)–(7) are their time-averaged values. According to the study of Ref. [6], the modeling results using the time-averaged approach (neglecting the density and temperature fluctuations) are almost the same as those obtained by using the density-weighted average approach under thermal plasma conditions. The effective 'diffusion' coefficients in Eqs. (2)–(7) are the combinations of their laminar and turbulent values, i.e., Γ_u, Γ_h, Γ_K and Γ_ε are calculated by

$$\Gamma_u = \mu + \mu_t; \quad \Gamma_h = k/c_p + \mu_t/Pr_t; \quad \Gamma_K = \mu + \mu_t/\sigma_K; \quad \Gamma_\varepsilon = \mu + \mu_t/\sigma_\varepsilon \tag{9}$$

where μ, k and c_p are the molecular viscosity, thermal conductivity, specific heat at constant pressure of the argon plasma, respectively. μ_t is the turbulent viscosity and is calculated by $\mu_t = \rho c_\mu K^2/\varepsilon$, whereas c_1, c_2, c_μ, σ_K, σ_ε and Pr_t are constants in the K–ε two-equation turbulence model, which are taken to be the values of 1.44, 1.92, 0.09, 1.0, 1.3 and 0.9, respectively. The data for the thermodynamic and transport properties of the argon plasma used in this paper are taken from Ref. [7].

2.3. Computational domain and boundary conditions

The computational domain used in this study is shown as ABCDEFGA in Fig. 2 with related geometrical sizes. The 0.5-mm-thick carrier-gas injection tube, with the inner radius and length of 4.0 and 5.0 mm, respectively, is included in the calculation domain. The inner radius of the torch nozzle exit (or the jet inlet, AB) is 4.0 mm. The distance between the frontal section of the carrier-gas injector and the plasma torch exit (L) is varied in this study for revealing its influences on the temperature and flow fields in the plasma reactor, while the length of the carrier-gas injection tube itself is kept constant. The outer free boundary (CD) is placed 40.0 mm away from the jet axis.

The boundary conditions employed in this study are as follows:

(i) At the torch nozzle exit (AB), $v_r = 0$, while the distributions for the plasma temperature and the axial velocity are specified as [8]:

$$T(r) = (T_0 - T_w)\left[1 - (r/R_{in})^4\right] + T_w \tag{10}$$

$$v_z(r) = v_{01}\left[1 - (r/R_{in})^4\right] \tag{11}$$

where T_w is the torch anode-nozzle inner-wall temperature (700 K is taken in this study), R_{in} is the inner radius of the torch nozzle. The maximum values of the temperature (T_0) and the axial velocity (v_{01}) on the centerline are taken according to the input power and the working-gas flow rate of the plasma torch with an assumed thermal efficiency. The turbulent kinetic energy K and its dissipation rate are assumed to be $K(r) = 0.005v_z^2$ and $\varepsilon(r) = 0.1K(r)^2$ [9].

(ii) At the inlet section of the carrier gas injector (EF), the gas temperature is specified in the range of 300–480 K in order to study the influence of the carrier-gas temperature on the heat transfer and flow patterns within the plasma reactor, whereas the axial velocity component is assumed to have the similar profile as that at the torch nozzle exit, i.e.,

$$v_z(r) = -v_{02}\left[1 - (r/R_{in})^4\right] \tag{12}$$

where v_{02} is the maximum absolute value of the axial velocity component at the centerline and calculated from the flow rate of the carrier gas. The radial velocity component, v_r, is set to be zero, and $K(r) = 0.005v_z^2, \varepsilon(r) = 0.1K(r)^2$ [9].

(iii) Along the solid walls (BC and DE), no-slip boundary condition is used for the velocity components, and the wall function method is employed for the turbulent flows [9]. The temperature distribution is assumed to be [10]:

$$T(r) = T_s - (T_s - T_{room})\frac{\ln(r/R_{in})}{\ln(R_{out}/R_{in})} \tag{13}$$

where R_{out} is the outer radius of the calculation domain ($R_{out} = 40.0$ mm), T_{room} is the room temperature (300 K), while T_s is the temperature at the inner points of the boundaries (at point B, $T_s = 700$ K; while at point E, T_s is varied from 300 to 480 K along with the variations of the carrier gas temperature), and $\partial\phi/\partial z = 0$ is employed for $\phi = K$ and ε.

(iv) At the jet axis (AF), axially symmetric conditions are employed, i.e., $v_r = 0$, and $\partial\phi/\partial r = 0$ for $\phi = v_z$, h, K, ε.

(v) Along the outer free boundary of the calculation domain (CD), zero-gradient boundary condition ($\partial\phi/\partial r = 0$) is employed for $\phi = v_z$, K and ε, and the mass conservation is satisfied for $\phi = v_r$, i.e., $\partial(\rho r v_r)/\partial r = 0$. For the gas temperature, if $v_r > 0$, $\partial T/\partial r = 0$; otherwise, $T = T_{room}$.

(vi) Inside the 0.5-mm-thick injection tube solid wall, the temperature is assumed to be equal the carrier-gas temperature.

In this paper, for revealing the effect of the swirling in the plasma jet or the carrier gas on the temperature and flow fields within the plasma reactor, it is assumed that the swirl velocity component takes the combined form of a solid vortex and a free vortex at the

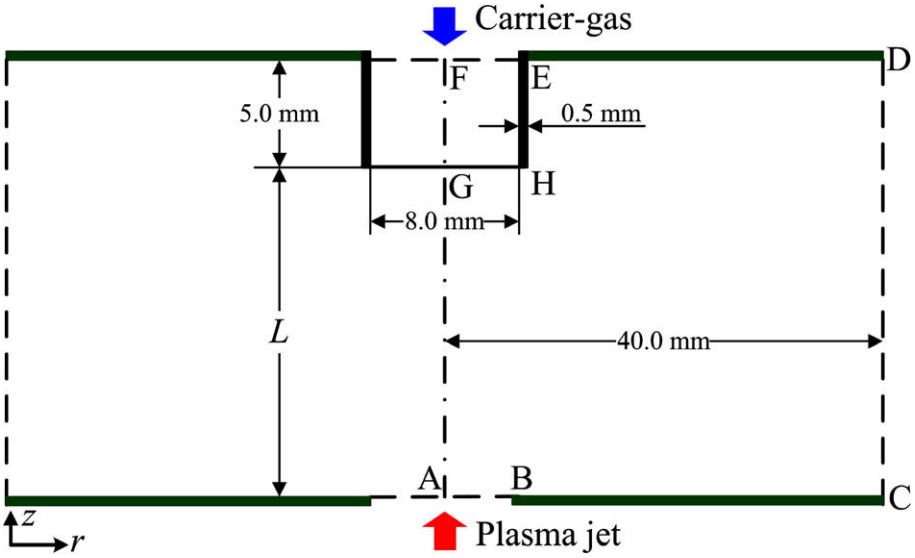

Fig. 2. Computational domain.

plasma jet inlet (AB) or the inlet of the carrier gas injector (EF) [11], i.e.,

$$|v_\theta(r)| = \begin{cases} v_{\theta m} r/R_s & 0 \leqslant r \leqslant R_s \\ v_{\theta m} \frac{R_s}{R_{in}-R_s}\left(\frac{R_{in}}{r}-1\right) & R_s < r \leqslant R_{in} \end{cases} \quad (14)$$

where $R_s = (2/3)R_{in}$, $v_{\theta m}$ is the maximum absolute value of the swirl velocity. $v_\theta(r) > 0$ or $v_\theta(r) < 0$ indicates that the direction of the swirl velocity is identical or opposite to the θ-direction. Correspondingly, the swirl number is calculated by $S = \left|\int_0^{R_{in}} \rho v_z v_\theta r^2 \, dr\right| / [R_{in} \times \int_0^{R_{in}} \rho v_z^2 r \, dr]|$ [11].

3. Modeling results and discussions

3.1. Calculation method

The SIMPLE algorithm [9,12] is used to solve the governing equations (1)–(7) simultaneously if the swirl flow exists in the plasma system. For the cases without swirling, v_θ is zero and Eq. (4) is not solved. In this study, for the cases of $L = 10.0$, 16.2 and 20.0 mm, two sets of non-uniform rectangular meshes with the grid points of 72 (z) × 102 (r), 82 (z) × 102 (r), 92 (z) × 102 (r) and 102 (z) × 152 (r), 122 (z) × 152 (r), 142 (z) × 152 (r) are employed for testing the grid dependence with $T_0 = 8500$ K, $v_{01} = 350$ m/s, $T_{car} = 450$ K and $v_{02} = 80$ m/s, respectively. The calculated results show that the corresponding relative discrepancies of the stagnation point positions using these two sets of meshes are all less than 3%. Thus, in the following studies, the non-uniform meshes (with finer mesh space near the walls and the centerline) with the grid points of 72 (z) × 102 (r), 82 (z) × 102 (r) and 92 (z) × 102 (r) are employed for the cases of $L = 10.0$, 16.2 and 20.0 mm, respectively, in order to save the CPU time.

3.2. Typical modeling results without swirl flows

The typical modeling results of temperatures and stream lines distributions within the plasma reactor are shown in Fig. 3 for the case of $T_0 = 8500$ K, $v_{01} = 350$ m/s, $T_{car} = 450$ K, $v_{02} = 90$ m/s (corresponding flow rate of the carrier gas is $Q_{car} = 114.0$ slpm) and $L = 16.2$ mm. It can be seen from Fig. 3 that due to the counter-injection of the carrier gas, a stagnation layer is formed between the plasma torch exit and the carrier-gas injector exit; the high-temperature partially-ionized gas is cooled down rapidly in the vicinity of the stagnation layer, which is helpful for controlling the particle coagulation and particle-particle coalescence processes, thereby maintaining small primary particle sizes in the nano-particle synthesis processes [5].

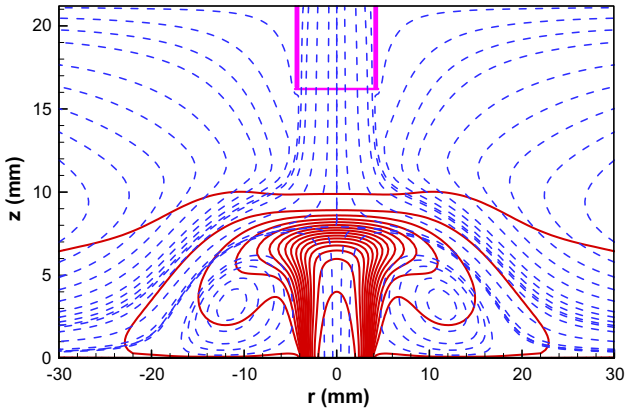

Fig. 3. Distributions of the calculated temperatures (solid lines, ranging from 500 to 8000 K with the interval of 500 K) and the stream lines (dashed lines) within the plasma reactor. $T_0 = 8500$ K, $v_{01} = 350$ m/s, $T_{car} = 450$ K, $v_{02} = 90$ m/s and $L = 16.2$ mm.

Keeping the inlet temperature and flow rate of the plasma jet, as well as the distance between the plasma torch exit and the carrier-gas injector exit, unchanged, the variations of the temperature and axial velocity component along the jet axis are shown in Figs. 4 and 5, respectively, for different carrier gas flow rates of $Q_{car} = 100.7$, 111.3 and 120.7 slpm (corresponding values of v_{02} are 75, 83 and 90 m/s at $T_{car} = 450$ K, respectively). If we define the stagnation point as the axial location with $v_z = 0$ at the jet axis, the predicted distances between the stagnation point and the plasma torch exit (λ) are 11.9, 9.8 and 7.9 mm, respectively, for the three carrier-gas flow rates shown in Figs. 4 and 5. It can also be seen from Figs. 4 and 5 that there exist steep gradients for the gas temperature and the axial velocity component in the vicinity of the stagnation layer; and with the increase of the carrier-gas flow rate, the stagnation layer is pushed toward the plasma torch exit due to the higher momentum of the counter-injected carrier gas being involved.

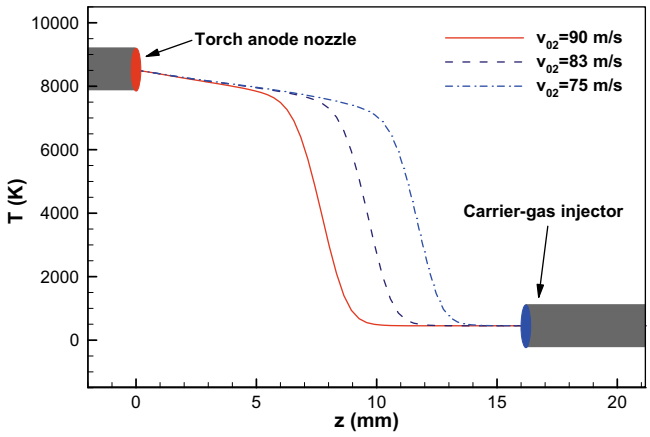

Fig. 4. Profiles of the gas temperature along the jet axis for different carrier-gas flow rates. T_0 = 8500 K, v_{01} = 350 m/s, T_{car} = 450 K and L = 16.2 mm.

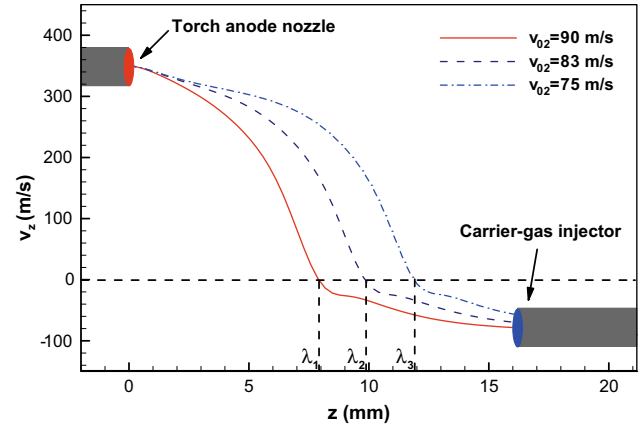

Fig. 5. Profiles of the axial velocity component along the jet axis for different carrier-gas flow rates. T_0 = 8500 K, v_{01} = 350 m/s, T_{car} = 450 K and L = 16.2 mm.

For comparing the relative positions of the stagnation layers under different operation conditions, a dimensionless parameter, $\xi = \lambda/L$, is defined in this study. The variations of ξ for different temperatures and flow rates of the carrier gas, with other parameters being unchanged, are shown in Fig. 6, which shows that with the decrease of the flow rate or the increase of the temperature of the carrier gas, the stagnation layer is pushed toward the carrier-gas injection tube due to the decrease of the momentum of the counter-injected carrier gas.

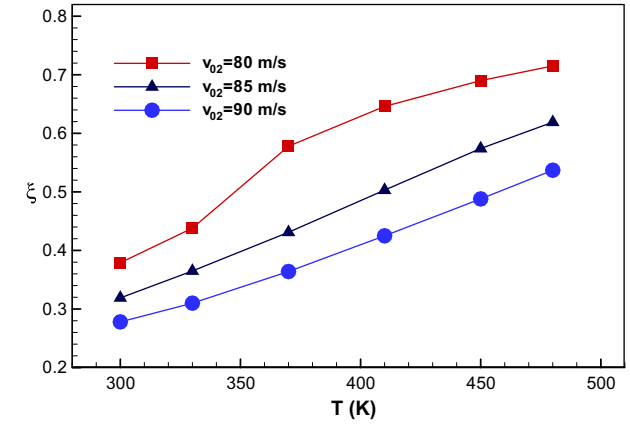

Fig. 6. Variations of ξ with the carrier-gas temperatures for three different carrier-gas injection velocities. T_0 = 8500 K, v_{01} = 350 m/s and L = 16.2 mm.

3.3. Effects of the input power of the plasma torch

The enthalpy and velocity of the plasma jet at the torch nozzle exit are related to the operation parameters of the plasma torch (i.e., the input power, the working-gas flow rate), and would affect the heat transfer and flow patterns within the plasma reactor significantly. In this sub-section, the relationship between the input power (P_{in}) of the plasma torch and the position of the stagnation layer is studied while other parameters, including the distance between the plasma torch exit and the carrier gas injector exit (L) and the temperature (T_{car}) and flow rate (Q_{car}) of the carrier gas, are kept unchanged. When different values of T_0 and v_{01} in Eqs. (10) and (11) are specified, the corresponding values of the plasma working-gas flow rates (Q_p) and the input and output powers of the plasma torch (P_{in} and P_{out}) can be obtained based on an assumed thermal efficiency of the plasma torch η = 0.4 [13]. The calculated values are listed in Table 1, where P_{out} represents the jet power at the plasma torch exit.

The predicted variations of the stagnation layer positions with the input powers of the plasma torch (in the range of P_{in} = 7.2–18.4 kW as listed in Table 1) are shown in Fig. 7 for three different carrier-gas injection velocities with L = 16.2 mm. It can be seen from Fig. 7 that (1) with the increase of the input power of the plasma torch, the stagnation layer is pushed toward the carrier-gas injection tube when other parameters (i.e., Q_{car}, T_{car}, L) are unchanged; and (2) especially for the case with smaller values of P_{in} (e.g., for P_{in} < 12.6 kW), the stagnation layer position changes significantly with the variation of the input power of the plasma torch. From Figs. 5–7, it can also be concluded that the stagnation layer between the plasma torch exit and the carrier-gas injector exit is formed due to the balance between the momentum of the plasma jet and that of the counter-injected gas flow. Hence, an appropriate combination of the operation parameters of the plasma torch and the carrier gas is necessary for obtaining a suitable stagnation layer position for the synthesis of nano-particles.

3.4. Effects of the distance between the plasma torch and the carrier-gas injector

The modeling results also show that besides the operation parameters of the plasma torch and the carrier gas (i.e., P_{in}, Q_p, T_{car}, Q_{car}), the distance between the plasma torch exit and the carrier gas injector exit (L) also significantly affects the location of the stagnation layer. The temperature and flow fields (v_{02} = 85 m/s), as well as the variations of λ, with the momenta of the carrier-gas corresponding to different values of L are shown in Fig. 8 for the case with T_0 = 8500 K, v_{01} = 350 m/s and T_{car} = 450 K. In Fig. 8(b), the momentum of the plasma jet or the cold carrier gas at its corresponding inlet section is defined as

$$M_i = 2\pi \int_0^{R_{in}} \rho v_z^2 r\,dr \quad (i = 1, 2) \tag{15}$$

where i = 1 or 2 represents the thermal plasma jet or the cold carrier gas. It can be seen from Fig. 8 that for the case with a larger value of

Table 1
List of the assumed values of the temperature (T_0) and axial velocity component (v_{01}) at the torch nozzle axis in Eqs. (10) and (11), and of the calculated argon flow rates, input and output powers of the plasma torch

v_{01} (m/s)	T_0 (K)	Q_p (slpm)	P_{out} (kW)	P_{in} (kW)
350	8500	34.0	2.86	7.15
400	9500	35.0	3.38	8.45
450	10,500	35.5	4.05	10.13
500	11,500	35.7	5.02	12.55
550	12,500	35.4	6.42	16.05
580	13,000	35.4	7.36	18.40

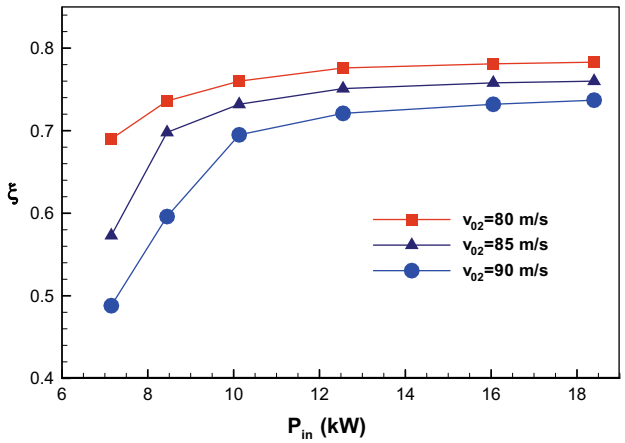

Fig. 7. Variations of ξ with the input powers of the plasma torch for three different carrier-gas injection velocities. T_{car} = 450 K and L = 16.2 mm.

L, the stagnation layer is somewhat easier to be pushed toward the plasma torch exit at higher carrier-gas flow rates; and the momentum ratio of the cold carrier gas to the thermal plasma jet ($R_M = M_2/M_1$) influences the positions of the stagnation layers (or the values of λ).

3.5. Swirling effects

In the preceding sub-sections, the effects of the swirling at the plasma jet inlet or the carrier-gas inlet on the heat transfer and flow patterns within the plasma reactor are not considered. In actual plasma processing, swirling flows always exist at the exit of the plasma torch because the plasma working-gas is usually admitted into the plasma torch with a swirl component in order to lighten the erosion of the anode nozzle during operation. Therefore, it is of importance to study the effect of swirling at the plasma jet or carrier gas side on the temperature and flow fields, as well as on the stagnation layer positions, within the plasma reactor. The predicted variations of the relative stagnation layer positions for the cases with the swirling at the plasma jet side ($S_1 = 0.1$, $S_2 = 0$) or at the carrier gas side ($S_1 = 0$, $S_2 = 0.1$) with T_0 = 8500 K, v_{01} = 350 m/s, T_{car} = 450 K and L = 16.2 mm are illustrated in Fig. 9(a), where the calculated results are also compared with those without swirl flows ($S_1 = S_2 = 0$). The corresponding distributions of the temperatures and streamlines for the case of v_{02} = 85 m/s are shown in Fig. 9(b). Fig. 9 demonstrates that when the temperatures and flow rates of the plasma jet and carrier gas (or the momentum of the thermal plasma jet and that of the carrier gas), as well as the distance between the plasma torch exit and the carrier-gas injector exit, are kept unchanged, the swirling motion of the plasma jet or the carrier gas retrains the axial flow of the fluids and leads to the change of the stagnation layer positions.

In the future, the existence of small amount of $AlCl_3$ vapor in the carrier gas, and the physical/chemical processes occurring in the vicinity of the stagnation layers, including the species diffusion, nucleation, coagulation, surface growth, particle motion and heating within the plasma reactor, should be considered. In addition, experimental measurements on the temperature and flow fields, as well as the distributions of the synthesized

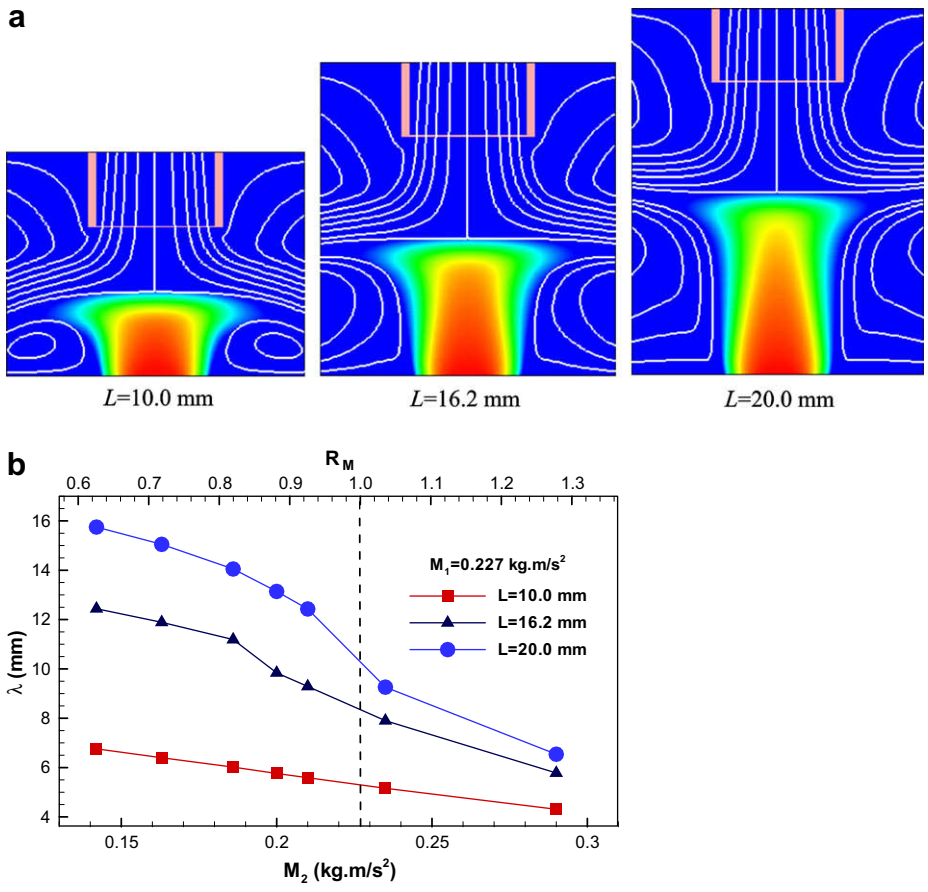

Fig. 8. Distributions of the calculated temperatures and streamlines within the plasma reactor with v_{02} = 85 m/s (a) and the variations of λ with the momentum of the carrier gas for different values of L (b). T_0 = 8500 K, v_{01} = 350 m/s and T_{car} = 450 K.

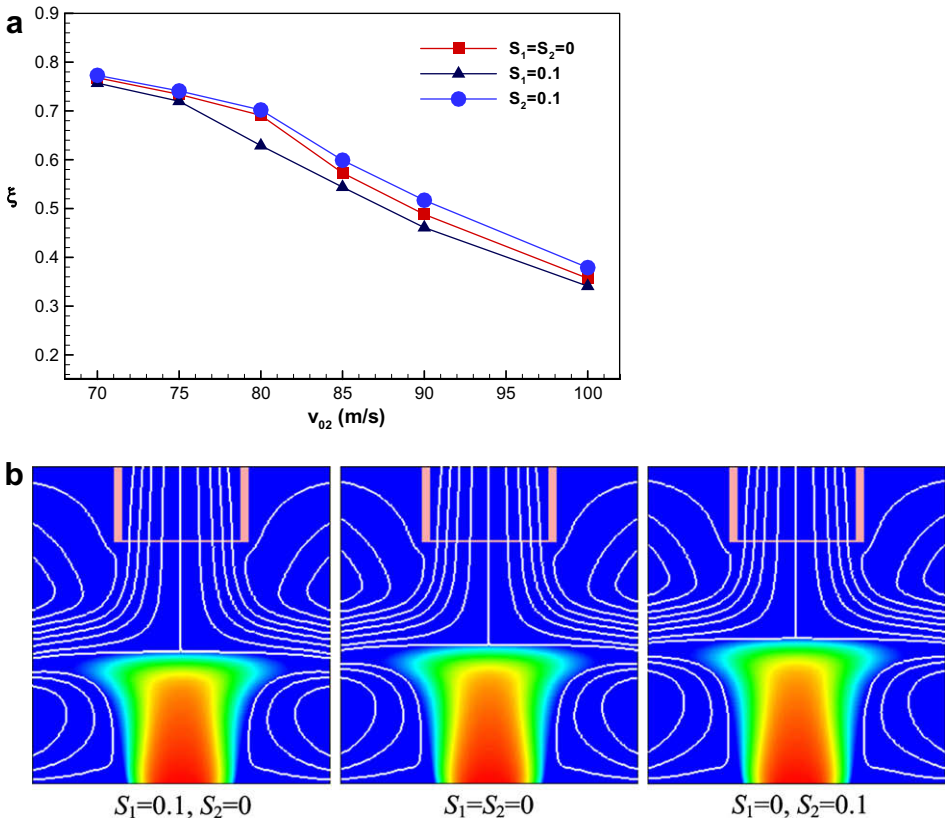

Fig. 9. Effects of the swirl flow on the relative positions of the stagnation layers (a) and the calculated temperatures and streamlines (b) within the plasma reactor for the case of v_{02} = 85 m/s. T_0 = 8500 K, v_{01} = 350 m/s, T_{car} = 450 K and L = 16.2 mm.

nano-particles, are also required to validate the physical/mathematical models by comparing the experimental and modeling results.

4. Concluding remarks

In this paper, modeling results are presented concerning the temperature and flow fields within a counter-injection plasma reactor. Due to the counter injection of the carrier gas opposite to the thermal plasma jet issuing from the plasma torch, a stagnation layer is formed between the plasma torch exit and the carrier-gas injector exit. The modeling results show that the heat transfer and flow patterns, as well as the locations of the stagnation layers, within the plasma reactor can be influenced significantly by many parameters including the flow rate (Q_{car}) and temperature (T_{car}) of the carrier gas (or the momentum of the carrier gas), the distance between the plasma torch exit and the carrier-gas injector exit (L), the input power (P_{in}) and flow rate (Q_p) of the plasma torch (or the momentum of the thermal plasma jet), and the swirling flow. Hence, an appropriate combination of the operation conditions of the plasma torch and the carrier gas is necessary for the counter-injection plasma reactor with a specified configuration (e.g., with a given distance L) to obtain a suitable stagnation layer position for the synthesis of nano-particles.

Acknowledgements

This work was supported by the National Natural Science Foundation of China (Nos. 10405015 and 50336010).

References

[1] E. Pfender, Thermal plasma technology: where do we stand and where are we going?, Plasma Chem Plasma Process. 19 (1) (1999) 1–31.
[2] X. Chen, Heat Transfer and Fluid Flow Under Thermal Plasma Conditions, Science Press, Beijing, 1993 (in Chinese).
[3] T.W. Or, P.C. Kong, E. Pfender, Counter-flow liquid injection plasma synthesis of spinel powders, Plasma Chem. Plasma Process. 12 (2) (1992) 189–201.
[4] S. Paik, X. Chen, P. Kong, E. Pfender, Modeling of a counterflow plasma reactor, Plasma Chem. Plasma Process. 11 (2) (1991) 229–249.
[5] B. Zhang, B. Liu, T. Renault, S.L. Girshick, M.R. Zachariah, Synthesis of aluminum nanoparticles using DC thermal plasma, in: J. Mostaghimi, T. Coyle, V.A. Pershin, H.R. Salimi Jazi (Eds.), Proceedings of the 17th International Symposium on Plasma Chemistry, Toronto, Canada, 2005, pp. 832–833.
[6] R. Ye, P. Proulx, M.I. Boulos, Turbulence phenomena in the radio frequency induction plasma torch, Int. J. Heat Mass Transfer 42 (1999) 1585–1595.
[7] A.B. Murphy, C.J. Arundell, Transport coefficients of argon, nitrogen, oxygen, argon–nitrogen, and argon–oxygen plasmas, Plasma Chem. Plasma Process. 14 (1994) 451–490.
[8] H.-P. Li, X. Chen, Three-dimensional modeling of the turbulent plasma jet impinging upon a flat plate and with transverse particle and carrier-gas injection, Plasma Chem. Plasma Process. 22 (1) (2002) 27–58.
[9] W.Q. Tao, Numerical Heat Transfer, second ed., Xi'an Jiaotong University Press, Xi'an, China, 2001 (in Chinese).
[10] R.L. Williamson, J.R. Fincke, D.M. Crawford, S.C. Snyder, W.D. Swank, D.C. Haggard, Entrainment in high-velocity, high-temperature plasma jets. Part II: computation results and comparison to experiment, Int. J. Heat Mass Transfer 46 (2003) 4215–4228.
[11] J.M. Beer, N.A. Chigier, Combustion Aerodynamics, Applied Science Publishing, London, 1972 (Section 5.1).
[12] S.V. Patankar, Numerical Heat Transfer and Fluid Flow, McGraw-Hill, New York, 1980.
[13] H.-P. Li, E. Pfender, X. Chen, Application of Steenbeck's minimum principle for three-dimensional modelling of DC arc plasma torches, J. Phys. D 36 (2003) 1084–1096.